ChemComm

COMMUNICATION

View Article Online
View Journal | View Issue

Cite this: *Chem. Commun.*, 2022, **58**, 5478

Received 15th February 2022,
Accepted 2nd April 2022

DOI: 10.1039/d2cc00949h

rsc.li/chemcomm

Phenylene as an efficient mediator for intermetallic electronic coupling†

Lyndsy A. Miller-Clark, Adharsh Raghavan, Reese A. Clendening and Tong Ren *

The new compound $[(NC)Ru_2(ap)_4]_2(\mu\text{-}1,4\text{-}C_6H_4)$ (ap = 2-anilinopyridinate) was prepared to address the open question of whether a 1,4-phenylene bridge can mediate intermetallic electronic coupling. As a manifestation of strong coupling, hole delocalization between the Ru_2 centers on the IR time scale (10^{-14} s) was established using spectroelectrochemistry. An orbital mechanism for coupling was elaborated with DFT analysis.

Conjugated organometallic compounds are promising building blocks for soft functional materials,[1–3] where the extensive dπ–π interactions render rich redox and optical properties unattainable in pure organic systems. Polymers based on metal–alkynyl units, polymetallaynes (**I** in Chart 1), are particularly attractive as electronic materials due to their structural rigidity, reduced band gaps and excellent charge mobility.[3–5] Correspondingly, the charge transfer processes across metal–acetylide backbones in mono- and bimetallic compounds have been extensively probed based on mixed-valency therein, and the structure–property relationships derived provide useful insight for material design.[6–8] Metal-acetylide motifs with proven proficiency in mediating charge transfer have been incorporated into nano-junctions with substantial conductance,[9,10] and have been shown to function as switches[11] and flash-like memory devices.[12] While the scope of metal–aryl chemistry is immense due to its relevance to cross coupling reactions,[13] polymetallaarylenes (**II** in Chart 1) have yet to be used for material applications. Furthermore, intermetallic coupling across a simple metal–(μ-1,4-phenylene)–metal backbone has never been experimentally demonstrated.

Diruthenium paddlewheel type compounds are well known for their robust redox responses.[14,15] Facile charge delocalization across the bridging oligoyn-diyl (C_{2n}) has been demonstrated in $[Ru_2(ap)_4]_2(\mu\text{-}C_{2n})$ type compounds (ap = 2-anilinopyridinate) through Vis-NIR spectroelectrochemical (SEC) experiments in bulk solutions.[16,17] The rich redox characteristics of Ru_2 compounds further enable a broad range of applications as wires in nano-junctions,[18,19] spin-chains,[20] and catalytic activation of small molecules.[21–23] More recently, $Ru_2(ap)_4(Ar)$ type compounds (Ar = aryl) were prepared,[24] and their capacity in binding small linear ligands such as CO, CN^- and C_2H^- at the axial site *trans*- to Ar was demonstrated.[25] Interested in expanding this chemistry to investigate bridging arylenes, we report herein the formation and characterization of $[Ru_2(ap)_4]_2(\mu\text{-}1,4\text{-}C_6H_4)$ (**1**, Scheme 1) and its derivative $[(NC)Ru_2(ap)_4]_2(\mu\text{-}1,4\text{-}C_6H_4)$ (**2**, Scheme 1), the unambiguous evidence of strong intermetallic coupling across the phenylene bridge through the SEC study of $[2]^+$, and companion DFT and TD-DFT analyses.

As detailed in the ESI,† the reaction of $Ru_2(ap)_4Cl$ with a slight excess of 1,4-dilithiobenzene yielded the phenylene bridged compound **1** (62%), and its 'dimeric' nature was verified by the isotopic distribution of Ru in the ESI-MS of **1** (Fig. S1, ESI†). Efforts to probe **1** spectroscopically were thwarted by its high sensitivity to air/moisture and low solubility in organic solvents. Seeking a more stable form of the dimer, **1** was treated with $[Bu_4N][CN]$ under N_2, which was followed by exposure to O_2 to yield **2** (59%). Compound **2**, a dimer of Ru_2(III,III) units, is air-stable and significantly more soluble than **1**. In order to benchmark electronic properties of **2**, the corresponding 'monomer' $(NC)Ru_2(ap)_4(C_6H_5)$ (**3**) was prepared from $Ru_2(ap)_4(C_6H_5)$[24] using the same procedure as for **2**.

Both the dimeric nature of **2** and the phenylene bridging are unambiguously established with the single crystal X-ray structure of **2** shown in Fig. 1, with key metric parameters also

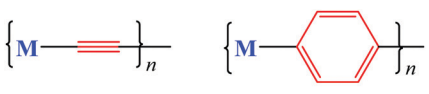

I II

Chart 1 Polymetallaynes(I) and polymetallaarylene(II) structural motifs.

Department of Chemistry, Purdue University, West Lafayette, Indiana 47907, USA. E-mail: tren@purdue.edu

† Electronic supplementary information (ESI) available: Spectroscopic data, and DFT and crystallographic details. CCDC 2149734–2149735. For ESI and crystallographic data in CIF or other electronic format see DOI: https://doi.org/10.1039/d2cc00949h

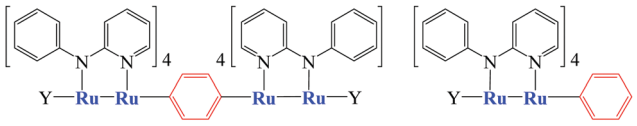

Scheme 1 Compounds discussed in this work.

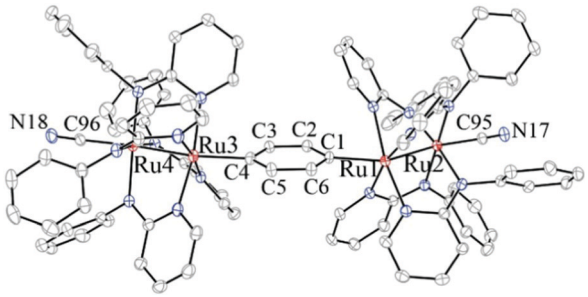

Fig. 1 ORTEP plot of **2** at 30% probability level. Selected bond lengths (Å) and angles (deg): Ru2–Ru1, 2.4892(3); Ru4–Ru3, 2.4829(3); Ru1–C1, 2.052(3); Ru3–C4 2.051(3); Ru2–C95, 2.019(3); Ru4–C96, 2.013(3); Ru2–Ru1–C1, 152.21(9); Ru4–Ru3–C4, 147.14(9); Ru1···Ru3, 6.95(4).

provided. The Ru_2 units in **2** display significant distortions from an idealized uniaxial paddlewheel structure as exemplified by the large deviation of Ru–Ru–C_{ph} from linearity, which is likely caused by a second order Jahn–Teller effect.[25] Both the Ru–Ru (*ca.* 2.49 Å) and Ru–C_{aryl} (*ca.* 2.05 Å) bond lengths closely match those found for the monomer **3** (Ru–Ru, 2.50 Å; Ru–C_{aryl}, 2.05 Å; Fig. S4 and Tables S1 and S2, ESI†), indicating similar electronic structures around the Ru_2 core between **2** and **3**.

Electronic coupling mediated by phenylene in **2** was first probed with voltammetric analysis. As shown in Fig. 2, compound **3** exhibits two reversible 1e$^-$ Ru_2-based couples: an oxidation **A** at 0.21 V (*versus* $Fc^{+/0}$) and a reduction **B** at −0.92 V, which is a characteristic common to Ru_2(III,III) species supported by the ap scaffold.[25,26] Compound **2** exhibits two 1e$^-$ oxidations at potentials close to that of **A** in 3 : 0.29 (**A2**) and 0.01 V (**A1**), and two 1e$^-$ reductions at potentials close to that of **B** in **3**: −0.91 (**B1**) and −1.09 V (**B2**). A reduction event (**C**) beyond **B2** is attributed to a species derived from degradation of $[2]^{2-}$. The stepwise appearance for the redox couples in **2** is a hallmark of significant intermetallic coupling through the bridging ligand.[27] Furthermore, the $\Delta E_{1/2}(+1)$ (calculated as: $E_{1/2}$(**A2**) − $E_{1/2}$(**A1**)) of **2**, 291 mV, is slightly higher than that reported for $[Ru_2(ap)_4]_2(\mu\text{-}C_2)$ (280 mV),[16] suggesting that the coupling in $[2]^+$ may be substantial. On the other hand, the $\Delta E_{1/2}(-1)$ ($E_{1/2}$(**B1**) − $E_{1/2}$(**B2**); 174 mV) of **2** is much smaller than that of $[Ru_2(ap)_4]_2(\mu\text{-}C_2)$ (660 mV) (further comparisons in Table S6, ESI†), hinting that the phenylene is less efficient in mediating coupling in $[2]^-$. It is worth mentioning that voltammograms of compound **1** (Fig. S5, ESI†), though less-than-ideal due to low solubility, also display the pattern of pairwise oxidations and reductions similar to that of **2**.

To quantify the degree of electronic coupling in **2**, mixed valency in both $[2]^+$ and $[2]^-$ were probed with Vis-NIR and IR

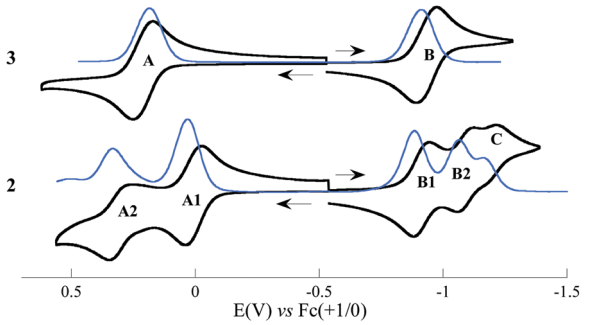

Fig. 2 Cyclic (black) and differential pulse (blue) voltammograms of compounds **2** and **3** (1.0 mM) recorded in 0.1 M Bu_4NPF_6 in THF at a scan rate of 0.100 V s^{-1}.

SEC experiments and compared with that of the monomer molecule, **3**. As shown in Fig. 3, both compounds **2** and **3** display an intense peak around 550 nm (18 350 cm^{-1}, band I), which is assigned to $\pi(Ru_2) \rightarrow \pi^*(N)/\delta^*(Ru_2)$.[28] Compound **3** also absorbs strongly around 950 nm (10 500 cm^{-1}, band II), and the analogous peak in **2** is shifted to 1025 nm (9900 cm^{-1}), which are likely the transitions between HOMO and LUMO ($\pi^*(Ru_2) \rightarrow \delta^*(Ru_2)$, see the DFT discussion below).

Upon the first 1e$^-$ reduction of **2**, both bands I and II are blue shifted with reduced intensities (Fig. S7a, ESI†). On the second 1e$^-$ reduction, both bands are further blue shifted with the former intensifying and the latter weakening (Fig. S7b, ESI†). Significantly, there is no discernible peak emerging in the red-NIR region, hinting at the localized nature of $[2]^-$ despite a sizable $\Delta E_{1/2}(-1)$. Furthermore, two distinctive ν(C≡N) (2092 and 2069 cm^{-1}) were located in the IR SEC of $[2]^-$ (Fig. S14, ESI†), which clearly confirms localization of the added electron on the IR time scale.[27]

Upon the first 1e$^-$ oxidation of **2**, both bands I and II are red shifted with II intensified. Very intriguingly, an intense new band (III) grows in with an onset around 5800 cm^{-1}. Because of the cutoff of the NIR spectrometer (2400 nm, 4167 cm^{-1}), only half of band III is recorded in the NIR SEC. Fortunately, much of the remaining half of band III is located in the IR SEC of $[2]^+$ (Fig. 3a and Fig. S12, ESI†), from which a nearly complete peak is constructed for band III. On the second 1e$^-$ oxidation, band III is completely bleached (Fig. 3b), while bands I and II further intensified. As a baseline study, the SEC of the first 1e$^-$ oxidation of **3** was recorded (Fig. 3c), where both bands I and II are red shifted with the latter slightly intensified, similar to those of $[2]^+$. Nonetheless, there is no new significant peak emerging for $[3]^+$ in the NIR–IR region. Hence, the absence of band III in both $[2]^{+2}$ and $[3]^+$ establishes it as an intervalence charge-transfer transition (IVCT).[6,27,29]

Further analysis of the IVCT band is enabled with Gaussian deconvolution of the Vis-NIR and IR SEC of $[2]^+$, which yields the following parameters for the fit (purple dash in Fig. 3a): $\bar{\nu}_{IVCT}$ = 4050 cm^{-1}, ε = 6860 M^{-1} cm^{-1}, $\Delta\bar{\nu}_{1/2}$ = 1716 cm^{-1} (Fig. S8–S11, ESI†). Importantly, the $\Delta\bar{\nu}_{1/2}$ is significantly smaller than the predicted value by the Hush model ($\Delta\bar{\nu}_{1/2}$ (Hush) = $(2310\ \nu_{IVCT})^{1/2}$ = 3060 cm^{-1}),[29] which, along with the large ε,

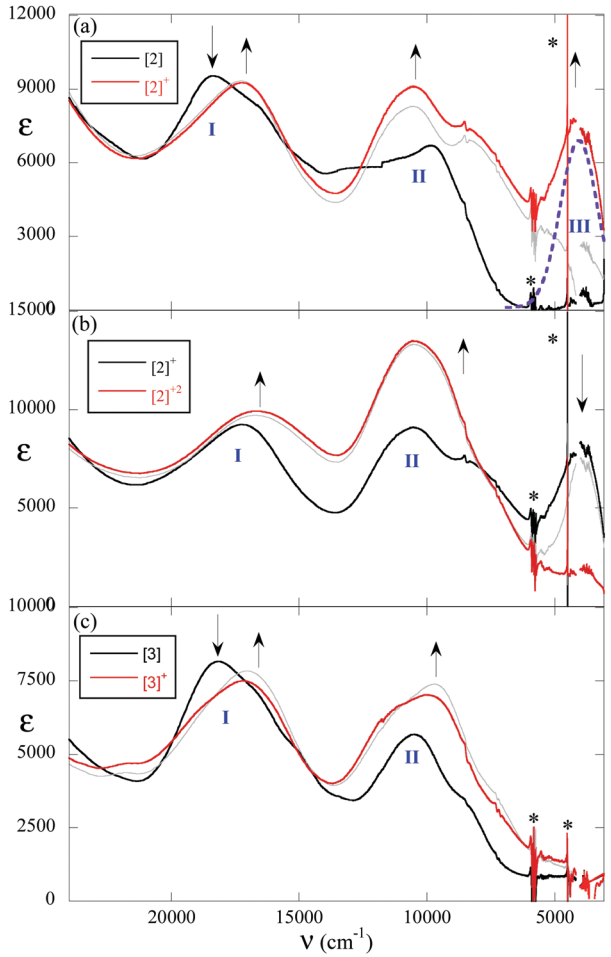

Fig. 3 Vis-NIR and IR spectroelectrochemistry of **2** with Gaussian fit of the IVCT band (purple dash) at 0.4 V (a), 0.65 V (b) and of **3** at 0.3 V (c) *vs.* Ag wire, 2 mM analyte with 0.1 M Bu_4NPF_6 in THF in all cases. Instrument artifacts/solvent overtones noted as * and grey lines used to denote intermediate scans for each SEC experiment.

suggests that $[2]^+$ is a highly delocalized (Robin-Day class III) mixed valence species. Further evidence cementing this assessment is the IR SEC of $[2]^+$ (Fig. S13, ESI†) that consists of a single and narrow C≡N stretch peak ($\Delta\bar{\nu}_{1/2} \sim 8$ cm^{-1}; in comparison, $\Delta\bar{\nu}_{1/2}$(C≡N) in $[3]^+ \sim 15$ cm^{-1} (Fig. S16, ESI†)), indicating that two Ru_2 cores are equivalent on the IR time scale (10^{-14} s).[27] The lower threshold of the electronic coupling element H_{AB} can be calculated based on the above mentioned IVCT band parameters and a Ru3···Ru1 distance (r) of 6.95 Å with the Mulliken–Hush equation:[6,29]

$$H_{AB} = (0.0206/r)(\bar{\nu}_{IVCT}\Delta\bar{\nu}_{1/2}\varepsilon)^{1/2} = 647 \text{ cm}^{-1}$$

To understand the underlying orbital mechanism for the observed Ru_2–Ru_2 coupling in $[2]^+$, DFT calculations were performed for **2**, $[2]^+$ and **3**. Our previous work[25] with (Y)$Ru_2(ap)_4(C_6H_4$–4-$NMe_2)$ indicated that the addition of axial ligands alters the ground state electron configuration (see note in ESI,† Fig. S20) from $\sigma^2\pi^4\delta^2(\pi^*\delta^*)^3$ in $Ru_2(ap)_4$(Ar) to either "$\pi^4\delta^2(\pi^*)^4$" (Y = CN) or "$\pi^4\delta^2(\pi^*)^4\delta^*$" (Y = CO). Magnetic susceptibility measurements using the Evans method[30] yielded effective magnetic moments at 293 K of 2.18 and 2.26μ_B for **2** and **3**, respectively (Table S8, ESI†). Both compounds contain $[Ru_2(ap)_4]^{2+}$ cores in the Ru_2(III,III) oxidation state, which is expected to be diamagnetic (S = 0 ground state). Population of a higher spin state (S = 1) is unusual for this class of compounds, but not unprecedented.[25,31] A possible explanation for this is an extensive mixing between a $[\pi_{xz}^2\pi_{yz}^2\delta^2(\pi_{xz}^*)^2(\pi_{yz}^*)^2]_2$ singlet and a $[\pi_{xz}^2\pi_{yz}^2\delta^2(\pi_{xz}^*)^2]_2(\pi_{yz,1}^*)^2\pi_{yz,2}^*\delta^*$ triplet (phenylene moiety is parallel to the xz plane). DFT calculations on **2** and **3** predicted a singlet–triplet energy gap of 0.87 kcal mol^{-1} and 2.0 kcal mol^{-1}, respectively. Such small barriers indicate that a large population of the triplet state may be feasible, or that the ground state has some multireference character.

Mulliken orbital composition analysis of the frontier orbitals of **2** (Fig. 4) reveals that its HOMO is primarily composed of the antibonding combination of π*(Ru–Ru) (62%) and π(Ph) orbitals (25%). On the other hand, the LUMO mainly consists of the δ*(Ru–Ru) on the Ru_2 cores (49% Ru contribution), with < 0.5% contribution from the bridging phenylene unit (Table S13, ESI†). DFT calculations on the 1e$^-$ oxidized $[2]^+$ predict an electronic configuration of "$[\pi_{xz}^2\pi_{yz}^2\delta^2(\pi_{xz}^*)^2]_2(\pi_{yz}^*)^3$" with the HOMO in **2** becoming the SOMO (singly occupied molecular orbital). The electronic configuration of $[2]^-$ is computed as $[\pi_{xz}^4\pi_{yz}^2\delta^2(\pi_{xz}^*)^2(\pi_{yz}^*)^2]_2\delta^*$ with the LUMO in **2** becoming the SOMO; the absence of phenylene contribution explains the lack of coupling in $[2]^-$. This accounts for the SEC observations: *i.e.*, $[2]^+$ exhibits an IVCT band in the NIR region, whereas $[2]^-$ does not.

Time-dependent DFT calculations (TD-DFT) on $[2]^+$ indicate that the observed IVCT band corresponds to a transition (calculated at 4647 cm^{-1}) from an orbital that is primarily a bonding combination of π*(Ru–Ru) (43.2% Ru d) and π(Ph) (7.2% C p_y) to the above-mentioned SOMO of $[2]^+$ (Fig. S21 and S22,

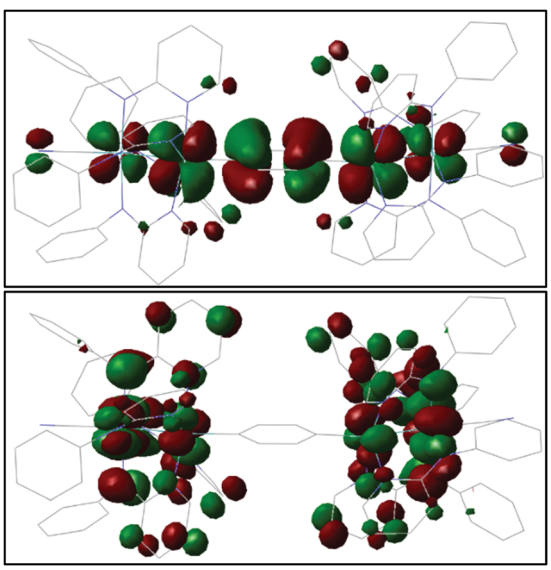

Fig. 4 HOMO (top) and LUMO (bottom) of the DFT-optimized structure of **2**. |Isovalue| = 0.020.

ESI†). In comparison, the previously studied $[Ru_2(ap)_4]_2(\mu\text{-}C_{2n})$ series ($[Ru_2(II,III)]_2$) have the localized δ* orbitals as SOMO/SOMO−1, while the antibonding combination of π*(Ru–Ru) and π(C≡C) are of lower energies.[16,17] Clearly, the phenylene ($C_6H_4^{2-}$) is a much stronger π-base ligand than oligoyn-diyl (C_{2n}^{2-}), and pushes π*(Ru–Ru) up to HOMO/SOMO, enabling intermetallic coupling by a mechanism different from those of M–C_{2n}–M.

In conclusion, two new phenylene-bridged compounds, $[(Y)Ru_2(ap)_4]_2(\mu\text{-}1,4\text{-}C_6H_4)$ (Y = nothing or CN^-), were prepared and characterized. Both Vis-NIR and IR SEC studies of $[\mathbf{2}]^+$ reveal its nature as a class III Robin-Day mixed valent ion with the hole being delocalized on the IR time scale (10^{-14} s). DFT analysis provides a rationale for the efficacy of the phenylene bridge in mediating hole transfer over electron transfer, while TD-DFT calculations reveal the origin of the IVCT band. While the intermetallic coupling mediated by arylene in a cyclo-metallated *N*,*C*,*N*-tridentate ligand was demonstrated in the pioneering studies of Sauvage and Launay,[32,33] this study provides the first unambiguous demonstration of strong coupling between metal units *via* plain phenylene bridge. In-depth understanding of magnetism, distance dependence, variation of ap backbone, and further DFT analysis are in the scope of future work.

The authors thank the National Science Foundation (CHE 2102049) for generously supporting this work, Prof. R. J. Crutchley for insightful discussion on SEC measurement and Mr Dan Clark for TOC design assistance.

Conflicts of interest

There are no conflicts to declare.

Notes and references

1 G. R. Whittell, M. D. Hager, U. S. Schubert and I. Manners, *Nat. Mater.*, 2011, **10**, 176–188.
2 A. Winter and U. S. Schubert, *Chem. Soc. Rev.*, 2016, **45**, 5311–5357.
3 V. W.-W. Yam, A. K.-W. Chan and E. Y.-H. Hong, *Nat. Rev. Chem.*, 2020, **4**, 528–541.
4 W.-Y. Wong and C.-L. Ho, *Acc. Chem. Res.*, 2010, **43**, 1246–1256.
5 C.-L. Ho, Z.-Q. Yu and W.-Y. Wong, *Chem. Soc. Rev.*, 2016, **45**, 5264–5295.
6 J.-P. Launay, *Chem. Soc. Rev.*, 2001, **30**, 386–397.
7 A. Haque, R. A. Al-Balushi, I. J. Al-Busaidi, M. S. Khan and P. R. Raithby, *Chem. Rev.*, 2018, **118**, 8474–8597.
8 M. R. Bryce, *J. Mater. Chem. C*, 2021, **9**, 10524–10546.
9 T. L. Schull, J. G. Kushmerick, C. H. Patterson, C. George, M. H. Moore, S. K. Pollack and R. Shashidhar, *J. Am. Chem. Soc.*, 2003, **125**, 3202–3203.
10 Y. Tanaka, Y. Kato, T. Tada, S. Fujii, M. Kiguchi and M. Akita, *J. Am. Chem. Soc.*, 2018, **140**, 10080–10084.
11 F. B. Meng, Y. M. Hervault, Q. Shao, B. H. Hu, L. Norel, S. Rigaut and X. D. Chen, *Nat. Commun.*, 2014, **5**, 3023Art. Number .
12 H. Zhu, S. J. Pookpanratana, J. E. Bonevich, S. N. Natoli, C. A. Hacker, T. Ren, J. S. Suehle, C. A. Richter and Q. Li, *ACS Appl. Mater. Interfaces*, 2015, **7**, 27306–27313.
13 D. Alberico, M. E. Scott and M. Lautens, *Chem. Rev.*, 2007, **107**, 174–238.
14 M. Cortijo, R. González-Prieto, S. Herrero, J. L. Priego and R. Jiménez-Aparicio, *Coord. Chem. Rev.*, 2019, **400**, 213040.
15 E. Van Caemelbecke, T. Phan, W. R. Osterloh and K. M. Kadish, *Coord. Chem. Rev.*, 2021, **434**, 213706Article.
16 G. L. Xu, G. Zou, Y. H. Ni, M. C. DeRosa, R. J. Crutchley and T. Ren, *J. Am. Chem. Soc.*, 2003, **125**, 10057–10065.
17 Z. Cao, B. Xi, D. S. Jodoin, L. Zhang, S. P. Cummings, Y. Gao, S. F. Tyler, P. E. Fanwick, R. J. Crutchley and T. Ren, *J. Am. Chem. Soc.*, 2014, **136**, 12174–12183.
18 A. S. Blum, T. Ren, D. A. Parish, S. A. Trammell, M. H. Moore, J. G. Kushmerick, G.-L. Xu, J. R. Deschamps, S. K. Pollack and R. Shashidhar, *J. Am. Chem. Soc.*, 2005, **127**, 10010–10011.
19 S. Ogawa, S. Chattopadhyay, Y. Tanaka, T. Ohto, T. Tada, H. Tada, S. Fujii, T. Nishino and M. Akita, *Chem. Sci.*, 2021, **12**, 10871–10877.
20 S. D. Su, X. Q. Zhu, Y. H. Wen, L. T. Zhang, Y. Y. Yang, C. S. Lin, X. T. Wu and T. L. Sheng, *Angew. Chem., Int. Ed.*, 2019, **58**, 15344–15348.
21 T. Miyazawa, T. Suzuki, Y. Kumagai, K. Takizawa, T. Kikuchi, S. Kato, A. Onoda, T. Hayashi, Y. Kamei, F. Kamiyama, M. Anada, M. Kojima, T. Yoshino and S. Matsunaga, *Nat. Catal.*, 2020, **3**, 851–858.
22 M. J. Trenerry, C. M. Wallen, T. R. Brown, S. V. Park and J. F. Berry, *Nat. Chem.*, 2021, **13**, 1221–1227.
23 J. F. Berry and C. C. Lu, *Inorg. Chem.*, 2017, **56**, 7577–7581.
24 A. Raghavan, B. L. Mash and T. Ren, *Inorg. Chem.*, 2019, **58**, 2618–2626.
25 A. Raghavan, F. Yuan and T. Ren, *Inorg. Chem.*, 2020, **59**, 8663–8666.
26 T. Ren, *Organometallics*, 2005, **24**, 4854–4870.
27 K. D. Demadis, C. M. Hartshorn and T. J. Meyer, *Chem. Rev.*, 2001, **101**, 2655–2686.
28 A. R. Corcos, M. D. Roy, M. M. Killian, S. Dillon, T. C. Brunold and J. F. Berry, *Inorg. Chem.*, 2017, **56**, 14662–14670.
29 B. S. Brunschwig, C. Creutz and N. Sutin, *Chem. Soc. Rev.*, 2002, **31**, 168–184.
30 D. F. Evans, *J. Chem. Soc.*, 1959, 2003–2005.
31 G. M. Chiarella, F. A. Cotton, C. A. Murillo, K. Ventura, D. Villagran and X. Want, *J. Am. Chem. Soc.*, 2014, **136**, 9580–9589.
32 J.-P. Sutter, D. M. Grove, M. Beley, J.-P. Collin, N. Veldman, A. L. Spek, J.-P. Sauvage and G. van Koten, *Angew. Chem., Int. Ed. Engl.*, 1994, **33**, 1282–1285.
33 C. Patoux, J.-P. Launay, M. Beley, S. Chodorowski-Kimmes, J.-P. Collin, S. James and J.-P. Sauvage, *J. Am. Chem. Soc.*, 1998, **120**, 3717–3725.